JNC TN9400 2002-079

Crack Opening Displacement of Circumferential Through-Wall Cracked Cylinders Subjected to Tension and In-Plane Bending Loads

January, 2003

O-ARAI ENGINEERING CENTER
JAPAN NUCLEAR CYCLE DEVELOPMENT INSTITUTE

JNC TN9400 2002-079
January, 2003

Crack Opening Displacement of Circumferential Through-Wall Cracked Cylinders Subjected to Tension and In-Plane Bending Loads

Yeon-Sik Yoo[1]

Abstract

This study is concerned with crack opening displacements (CODs) of cylinders with a circumferential through-crack which is subjected to tension and in-plane bending loads. Most studies about crack opening behavior have performed on membrane and global bending stresses. Moreover, they cannot be valid for large-scale structures. For simplicity on evaluation for structural integrity, crack opening displacement has been often calculated by plate or pipe model considering almost stresses as a membrane component. However, it is important to investigate ones close to real crack opening behaviors under stress states for reliability on evaluation. The results must be directly related to evaluate leakage detection in reactor vessel and the primary piping system of FBR structures. From that purpose, a series of FEM analyses were performed, and hence the characteristics of COD under an in-plane bending stress were compared with those under a membrane stress. In addition, the plate model was indicated to be unreasonable for application on large-scale pipes by comparing the plate model with the pipe model. The results of this study are expected to be valid for leakage evaluation of high temperature structures especially.

[1] Structural Mechanics Research Group, Advanced Technology Division, Oarai Engineering Center

引張と板曲げ荷重を受ける周方向貫通き裂を有する管でのき裂開口変位

兪　淵植

要　旨

この研究は、引張と板曲げ荷重を受ける周方向貫通き裂を有する管でのき裂開口変位に関するものである。き裂開口変位に関する従来の研究例では、主に引張荷重及び管曲げ荷重を考慮した。また、大型構造物に対してはその適用範囲を超える場合が多い。構造健全性評価の際、簡単のためしばしば殆どの応力が膜成分として取り扱われ、平板あるいは配管モデルによってき裂開口変位が評価される。しかしながら、評価の信頼性のためには応力状態により近いき裂開口挙動を調べることは重要である。その成果は、FBR構造物の炉容器及び1次配管系における漏洩検知評価に緊密に関係することとなる。このような趣旨で、本研究では一連の有限要素解析が実施され、板曲げ応力によるき裂開口変位の特徴と膜応力によるき裂開口変位の特徴が調べられた。なお、平板モデルと配管モデルでの違いを比較することによって、大型配管問題における平板モデルの適用の不合理性を指摘した。本研究の成果は特に高温構造物における漏洩評価への適用が期待される。

CONTENTS

Tables List

Figures List

1. Introduction

In the origin of the assurance of structural integrity, energy-related structures such as nuclear power plants should have the capability to detect the enough leakage of coolant in a short period in order to protect the severe fracture in an emergency, to that purpose, a great importance was recently attached to the accurate detection of leakage. The proper evaluation methods related to crack opening behavior after crack penetration have been studied in many aspects. However, most studies about crack opening behavior have performed on membrane and global bending stresses which were induced from internal pressure and thermal expansion respectively.

On the other hand, some severe parts in nuclear power plants are subjected to large in-plane bending stresses in addition to membrane stresses. The basic concept on crack opening behavior due to the in-plane bending stress originates in that the effects on the COD of the membrane and the in-plane bending stresses are different indubitably. Thus, it is necessary to evaluate the COD due to the in-plane bending load in cylinders, considering the integrity of structures subjected to severe service condition under high temperature.

It is also important for noticing that minimum crack length on through-wall crack surface mainly controls coolant leakage. Therefore, crack opening behavior should be assessed not only in the centre of thickness but in inner and outer surfaces considering the corresponding loading conditions.

This study clarified the effect of membrane and bending stresses on the COD of a circumferential through-wall cracked cylinder by caring out FEM analyses, and as results the CODs were arranged considering crack length and cylinder geometry.

2. Evaluation of COD

2.1 Evaluation model

The FEM models were constructed by 20-nodes solid elements which have degrees of freedom of displacements to x, y and z. The infinite solid condition was applied to the models by taking the axial length, 2H, as twice the perimeter, $2\times2\pi R$, considering that most evaluation objects in the RV and the piping structure satisfy the infinite condition. The FEM models were composed of 1/4 models on the basis of structural symmetry. Figure 1 shows the model of half crack angle of 10 degree and R/t of 10 as an example. The analysis code was FINAS (Finite Element Nonlinear Structural Analysis System) Ver.15 [1]. Two aspects of the membrane and inner-surface plus-bending stresses and the membrane and outer-surface plus-bending stresses were set for analyses. All analyses were performed under the membrane stress as the first step, and the in-plane bending stress as the second step. The membrane and the plus-bending stresses were set to be equal in order to investigate the effect of minus-bending stress which has an equivalent absolute value to plus-bending stress on crack closure. The schematic loading types were illustrated in Fig.2.

2.2 Crack opening behavior of cylinder under a membrane stress

The crack opening behavior of through crack has a significant meaning for evaluating the structural integrity. As one of the representative parameters on crack opening behavior of cylinder typed structures, the COD concept is widely used. The COD of a circumferential through-wall cracked cylinder can be evaluated by assuming a proper crack shape from the COA (crack opening area) evaluation method proposed by Tada-Paris [2].

Tada-Paris equation

$$A_m = \frac{\sigma_m}{E}\left(\pi R^2\right) I_m(\theta) \qquad (1)$$

At R/t=10

$$I_m(\theta) = 2\theta^2\left[1+\left(\frac{\theta}{\pi}\right)^{\frac{3}{2}}\left\{8.6-13.3\left(\frac{\theta}{\pi}\right)+24\left(\frac{\theta}{\pi}\right)^2\right\}\right.$$
$$\left.+\left(\frac{\theta}{\pi}\right)^3\left\{22.5-75\left(\frac{\theta}{\pi}\right)+205.7\left(\frac{\theta}{\pi}\right)^2-247.5\left(\frac{\theta}{\pi}\right)^3+242\left(\frac{\theta}{\pi}\right)^4\right\}\right] \quad (2)$$

$$\delta_m = \frac{2A_m}{\pi c} \quad (3)$$

$$c = \theta R \quad (4)$$
$$(0 < \theta < 100^o)$$

Where, θ denotes half crack angle, R is mean radius of a cylinder, t is wall thickness and c is half crack length. All parameters with subscript m denote results subjected to a membrane stress.

GE/EPRI equation [3] gives another reasonable solution to the COD evaluation of cylinders.

GE/EPRI equation

$$\delta_m = \frac{4\sigma_m c}{E} V_m\left(\frac{\theta}{\pi}, \frac{R}{t}\right) \quad (5)$$

$$V = 1 + A\left[4.55\left(\frac{\theta}{\pi}\right)^{1.5} + 47.0\left(\frac{\theta}{\pi}\right)^3\right] \quad (6)$$

$$A = \left[0.125\left(\frac{R}{t}\right)-0.25\right]^{0.25} \qquad 5 \le \frac{R}{t} \le 10 \quad (7)$$
$$A = \left[0.4\left(\frac{R}{t}\right)-3.0\right]^{0.25} \qquad 10 \le \frac{R}{t} \le 20$$
$$(0 \le \theta/\pi \le 0.5)$$

The above two methods, however, should be ascertained their reasonableness in the COD evaluation of the large-scale structure. On that reason, this study treated the COD evaluation method applicable to the large-scale structures which have R/t over 20. From a series of FEM analyses, the following normalized CODs that would correspond to $V_m(\theta/\pi,R/t)$ of Eq.(5) were arranged at inner, mean and outer-surface of cracks separately:

$$V_m^{in}\left(\frac{\theta}{\pi},\frac{R}{t}\right)=\frac{\delta_m E}{4\sigma_m c_{in}} \tag{8}$$

$$V_m^{mean}\left(\frac{\theta}{\pi},\frac{R}{t}\right)=\frac{\delta_m E}{4\sigma_m c_{mean}} \tag{9}$$

$$V_m^{out}\left(\frac{\theta}{\pi},\frac{R}{t}\right)=\frac{\delta_m E}{4\sigma_m c_{out}} \tag{10}$$

As the results of fitting from FEM analyses, the normalized COD parameter $V_m(\theta/\pi,R/t)$ of eq.(8) to (10) were obtained as the table 1 to 3.

The normalized CODs from FEM analysis results for Eq.(8) to (10) were compared with those from the above two solutions in Fig.3. On the whole, the present FEM results show a good agreement with the theoretical solutions. The differences with Tada-Paris solution may result from an assumption that a crack opening shape was assumed as an ellipse. At the normalized half crack angle below 0.0556 in Fig.3, the CODs through the wall thickness show very complex behaviors. That imply the COD of small crack does not satisfy plane stress condition even if a cylinder has a thin wall thickness. Therefore, it is considered that close attention is paid to the assessment of the COD in small cracks. Application of plane strain condition may help this problem partially, with giving a proper answer in engineering. In addition, if considering that crack in the location where penetration is expected to be occurred primarily controls the leakage detection, general mean-radius based approaches may induce its unreliability on leakage evaluation and this phenomenon is considered to be dominantly shown in small cracks.

In this study, the COD behaviors were arranged with a consistency using the modulus of elasticity, E, regardless of the inner, mean and outer-surfaces of cracks because an application of the plane strain condition at mean-surface seems not to give good COD solutions in large cracks.

2.3 Crack opening behavior of cylinder under an in-plane bending stress

As the second step, two aspects of plus-bending stress at inner and outer-surface in addition to the first step such as Sec.2.2 were considered as Fig.2. The basic forms on the normalized COD due to bending stress was separated into each aspect with the similarity to Eq.(8) and (10).

$$V_b^{in}\left(\frac{\theta}{\pi},\frac{R}{t}\right)=\frac{\delta_b E}{4\sigma_b c_{in}} \quad (11)$$

$$V_b^{out}\left(\frac{\theta}{\pi},\frac{R}{t}\right)=\frac{\delta_b E}{4\sigma_b c_{out}} \quad (12)$$

Simultaneously, the parameters $V_b(\theta/\pi,R/t)$ of Eq.(11) and (12) were also arranged as the table 4 and 5 based on FEM analyses.

Crack opening behaviors of inner and outer-surfaces subjected to a plus-bending stress were precisely illustrated in Fig.4 and Fig.5 respectively. In Fig.4, the V_b^{in} (θ/π, R/t) values show the inclination to decrease below zero as a crack angle becomes to be large in spite of under plus-bending states, which implies the effect of minus-bending stress at outer-surface is much prominent as crack length becomes great. On the other hand, the V_b^{out} (θ/π, R/t) in Fig.5 is considered to show behaviors similar to a plate.

2.4 Crack opening behavior of cylinder under a membrane and an in-plane bending stresses

From the present FEM analyses, crack opening behavior of cylinder under a membrane and an in-plane bending stress was investigated. Figure 6 shows comparisons between the parameter $V_m(\theta/\pi,R/t)$ due to a membrane stress and $V_b(\theta/\pi,R/t)$ due to a plus-bending stress at inner and outer-surfaces respectively. As seen in that figure, the effect of an in-plane bending stress on crack opening behavior is much less than an equivalent valued membrane stress. Additionally, these results are apparently inclined to be shown at inner-surface. Considering leakage detection of structure, crack opening behavior should be required regardless of any stress states. Figure 7 and 8 show the effects of a membrane and an in-plane bending stress on a crack opening displacement at inner and outer-surface of cylinder respectively. Entirely, at the larger R/t, it is confirmed that in-plane bending stress contributes less on crack opening behavior. From Fig.7 and 8, at last, the lower part of each evaluation lines must correspond to the region inducing crack opening behavior. Using the present results, the COD as a requisition for leakage detection on RV and pipes subjected to membrane and in-plane bending stresses is expected to be evaluated reasonably.

3. Application

The results of this study can be applied for the COD evaluation of an advanced loop typed large-scale LMFR (Liquid Metal Fast-breeder Reactor). The objects on evaluation were set to around sodium surface of RV (reactor vessel); thermal stressed piping system and so on. Especially, the vicinity of the sodium surface of RV is generally considered to be a severe on assessment of structural integrity on account of the fluctuations of coolant temperature and sodium surface.

In this study, the following large-scale LMFR was considered as an application example [4]: inner diameter (I.D.) = 9600mm, thickness (t) = 30mm, R/t = 160.

Assuming a circumferential crack around the sodium surface, the axial stress components from the design values of LMFR are arranged as Table 6.

From Table 6, the axial membrane and bending stresses can be summarized as follows:

$$\sigma_m = 31.0 \text{ MPa} \quad (13)$$

$$\sigma_b = 75.0 \text{ MPa} \quad (14)$$

Using the above stress conditions, a limit crack size which makes the coolant leakage detected may be also calculated.

From Fig.9, if stress conditions are subjected to Eq.(13) and (14) in the inner or outer-surface of the RV respectively, θ/π for leakage detection obtained from the present study requires above 0.01, though the plate model gives 0.67. Moreover, if considering the membrane stress only is restricted to Eq.(13), the in-plane bending stress which induce crack opening in a certain crack length can be evaluated in this figure.

4. Discussion

It is necessary for noticing that the opening behaviors of circumferential crack in the cylinder are obviously different from those in the plate. Circumferentially through-wall cracked cylinder seems to have rotation even due to a tension. Occasionally, a cylinder with a large R/t has been often misled to show the COD behavior similar to a plate. This study is, however, to certify that the larger a cylinder has R/t, under a membrane stress, a crack shows the greater opening behavior than a plate and hence the less an in-plane bending stress affects on the COD.

5. Conclusion

Crack opening displacements of circumferential through-wall cracked cylinders subjected to a membrane and an in-plane bending stress were investigated by a series of FEM analyses in this study. The differences of crack opening behavior between plate and cylinder were also discussed. The present results are expected to be usefully applied for evaluation of leakage detection in the thin-walled reactor vessel and the pipes subjected to transient states. Especially, LMFR structures which are operated under low internal pressure and high temperature are considered to be good objects for application of the present results.

Acknowledgement

The author would like to express his sincere thanks to Mr. Hideo Machida of TEPCO SYSTEMS CORPORATION who gave major and beneficial advices on this study.

References

1. FINAS ver.15.0, "Users's Manual", PNC TN9520 95-014(1995)
2. H. Tada, P. C. Paris. "The Application of Fracture Proof Design Methods Using Tearing Instability Theory to Nuclear Piping Postulating Circumferential Through Wall Cracks", NUREG/CR-3464 (1983)
3. K. Kishida, A. Zahoor. "Crack Opening Area Calculations for Circumferential Through-Wall Pipe Cracks", EPRI NP-5959-SR.T (1988)
4. T. Mihara, et al., "Feasibility Studies on Fast Breeder Reactor Plant Systems", Japan Nuclear Cycle Development Institute, TY9400 2001-012 (2001)

Table 1 Normalized COD parameter $V_m^{in}(\theta/\pi, R/t)$ under a membrane stress

R/t / θ/π	5	10	15	20	25	30	35	40	45	50	60	70	80	90	100	120	140	160
0.0056	1.0604	1.0614	1.0507	1.0395	1.0292	1.0199	1.0115	1.0043	0.9981	0.9927	0.9883	0.9796	0.9743	0.9705	0.9677	0.9640	0.9613	0.9594
0.0139	1.0814	1.0485	1.0239	1.0069	0.9955	0.9878	0.9825	0.9786	0.9757	0.9735	0.9702	0.9681	0.9665	0.9656	0.9648	0.9643	0.9644	0.9650
0.0278	1.0623	1.0131	0.9910	0.9806	0.9754	0.9727	0.9717	0.9715	0.9722	0.9734	0.9768	0.9815	0.9869	0.9931	0.9997	1.0142	1.0297	1.0460
0.0556	1.0352	0.9974	0.9943	1.0012	1.0128	1.0269	1.0426	1.0592	1.0767	1.0945	1.1308	1.1677	1.2057	1.2435	1.2812	1.3566	1.4312	1.4984
0.1111	1.0788	1.1121	1.1778	1.2531	1.3318	1.4113	1.4903	1.5682	1.6447	1.7196	1.8772	2.0056	2.1406	2.2766	2.3983	2.6408	2.8593	3.0912
0.1667	1.2370	1.3823	1.5536	1.7325	1.9119	2.0887	2.2610	2.4276	2.5882	2.7433	3.0269	3.2957	3.5770	3.8424	4.0822	4.4954	4.9294	5.3444
0.2222	1.5063	1.8005	2.1077	2.4208	2.7332	3.0407	3.3399	3.6283	3.9049	4.1707	4.6509	5.1280	5.5310	6.0301	6.4192	7.1533	7.9020	8.7700
0.2778	1.9065	2.3900	2.8672	3.3519	3.8425	4.3341	4.8207	5.2963	5.7578	6.2045	7.0162	7.8100	8.4831	9.2725	10.0204	11.4772	13.0093	14.4112
0.3333	2.4814	3.2036	3.8919	4.5980	5.3325	6.0921	6.8660	7.6429	8.4138	9.1738	10.5834	11.9854	13.1728	14.5794	16.1455	18.5856	21.3439	24.3678
0.3889	3.3099	4.3374	5.2939	6.2930	7.3666	8.5160	9.7277	10.9823	12.2626	13.5564	15.9762	18.8114	21.3212	23.3722	26.3708	31.2299	36.1216	41.3609
0.4444	4.5304	5.9589	7.2712	8.6658	10.2075	11.9095	13.7591	15.7316	17.8014	19.9502	24.1896	29.2253	32.9683	38.0534	41.8999	52.3207	61.5136	70.9622
0.5	6.3908	8.3712	10.1771	12.1175	14.2983	16.7549	19.4840	22.4627	25.6638	29.0652	36.6449	43.3933	51.1535	60.8021	68.5499	86.3398	103.7574	121.7375

Table 2 Normalized COD parameter $V_m^{mean}(\theta/\pi, R/t)$ under a membrane stress

θ/π \ R/t	5	10	15	20	25	30	35	40	45	50	60	70	80	90	100	120	140	160
0.0056	0.8795	0.8930	0.9028	0.9133	0.9231	0.9316	0.9387	0.9446	0.9494	0.9533	0.9604	0.9652	0.9671	0.9688	0.9705	0.9732	0.9753	0.9771
0.0139	0.9170	0.9444	0.9643	0.9768	0.9848	0.9902	0.9942	0.9974	1.0003	1.0027	1.0072	1.0113	1.0150	1.0187	1.0222	1.0290	1.0357	1.0423
0.0278	0.9552	0.9906	1.0073	1.0179	1.0266	1.0344	1.0417	1.0488	1.0558	1.0625	1.0757	1.0886	1.1012	1.1139	1.1263	1.1508	1.1749	1.1983
0.0556	1.0162	1.0560	1.0852	1.1123	1.1384	1.1639	1.1887	1.2131	1.2369	1.2604	1.3058	1.3502	1.3942	1.4364	1.4780	1.5591	1.6378	1.7108
0.1111	1.1486	1.2502	1.3444	1.4364	1.5260	1.6131	1.6973	1.7791	1.8581	1.9350	2.0894	2.2213	2.3546	2.4866	2.6070	2.8432	3.0479	3.2808
0.1667	1.3471	1.5535	1.7467	1.9364	2.1219	2.3018	2.4751	2.6415	2.8008	2.9537	3.2302	3.4913	3.7641	4.0172	4.2523	4.6576	5.0818	5.4885
0.2222	1.6314	1.9802	2.3030	2.6215	2.9353	3.2416	3.5380	3.8226	4.0946	4.3552	4.8265	5.2920	5.7366	6.1743	6.5598	7.3860	8.1884	8.8913
0.2778	2.0297	2.5634	3.0497	3.5348	4.0228	4.5104	4.9923	5.4631	5.9189	6.3604	7.1676	7.9540	8.7036	9.4353	10.1514	11.6018	13.1385	14.5340
0.3333	2.5885	3.3590	4.0509	4.7537	5.4840	6.2399	7.0104	7.7843	8.5520	9.3101	10.7254	12.1282	13.3359	14.7916	16.2742	18.7259	21.4821	24.4916
0.3889	3.3854	4.4627	5.4199	6.4144	7.4854	8.6341	9.8468	11.1030	12.3852	13.6825	16.1300	18.9394	21.6337	24.0696	26.5092	31.3806	36.2640	41.3690
0.4444	4.5534	6.0401	7.3540	8.7471	10.2905	11.9966	13.8531	15.8335	17.9118	20.0710	24.3600	28.8673	33.4305	38.3054	43.0333	52.4706	61.6353	70.9246
0.5	6.3288	8.3875	10.2031	12.1478	14.3372	16.8043	19.5478	22.5427	25.7588	29.1818	36.7780	43.7024	52.0084	60.3716	68.7728	86.3573	103.5826	121.4530

Table 3 Normalized COD parameter $V_m^{out}(\theta/\pi, R/t)$ under a membrane stress

θ/π \ R/t	5	10	15	20	25	30	35	40	45	50	60	70	80	90	100	120	140	160
0.0056	1.0578	1.0566	1.0492	1.0413	1.0340	1.0274	1.0215	1.0166	1.0124	1.0089	1.0081	1.0025	1.0000	0.9989	0.9986	0.9995	1.0012	1.0033
0.0139	1.0657	1.0524	1.0427	1.0374	1.0357	1.0363	1.0384	1.0412	1.0444	1.0479	1.0550	1.0622	1.0691	1.0761	1.0828	1.0958	1.1083	1.1204
0.0278	1.0574	1.0559	1.0649	1.0779	1.0916	1.1051	1.1179	1.1304	1.1423	1.1537	1.1755	1.1960	1.2155	1.2342	1.2522	1.2864	1.3188	1.3495
0.0556	1.0807	1.1323	1.1808	1.2237	1.2628	1.2988	1.3325	1.3643	1.3945	1.4235	1.4783	1.5296	1.5797	1.6264	1.6717	1.7585	1.8414	1.9129
0.1111	1.2263	1.3799	1.5021	1.6115	1.7129	1.8082	1.8987	1.9846	2.0668	2.1458	2.2992	2.4324	2.5639	2.6918	2.8105	3.0403	3.2461	3.4660
0.1667	1.4447	1.7091	1.9281	2.1316	2.3251	2.5096	2.6852	2.8521	3.0105	3.1617	3.4295	3.6819	3.9478	4.1922	4.4190	4.8130	5.2278	5.6266
0.2222	1.7365	2.1422	2.4858	2.8132	3.1304	3.4372	3.7320	4.0133	4.2807	4.5365	4.9976	5.4515	5.8387	6.3128	6.6942	7.4175	8.1482	9.0025
0.2778	2.1308	2.7190	3.2204	3.7092	4.1969	4.6821	5.1601	5.6262	6.0766	6.5127	7.3129	8.0922	8.7670	9.5296	10.2729	11.7130	13.2208	14.6265
0.3333	2.6749	3.4979	4.1994	4.9022	5.6310	6.3838	7.1521	7.9229	8.6871	9.4425	10.8592	12.2620	13.4737	14.8421	16.3885	18.8431	21.5640	24.5772
0.3889	3.4450	4.5742	5.5375	6.5309	7.6013	8.7503	9.9644	11.2222	12.5050	13.8043	16.2673	19.0558	21.4958	23.7686	26.6270	31.4819	36.3242	41.5040
0.4444	4.5691	6.1116	7.4317	8.8253	10.3719	12.0838	13.9476	15.9359	18.0210	20.1882	24.5113	29.3261	33.2618	38.5234	42.2784	52.4791	61.5609	70.9255
0.5	6.2743	8.4011	10.2271	12.1785	14.3777	16.8582	19.6163	22.6272	25.8574	29.2972	36.9040	43.9571	51.9087	61.4225	68.6571	86.1272	103.3726	121.1100

Table 4 Normalized COD parameter $V_b^{in}(\theta/\pi, R/t)$ under an in-plane bending stress

θ/π \ R/t	5	10	15	20	25	30	35	40	45	50	60	70	80	90	100	120	140	160
0.0056	0.9836	0.9132	0.8470	0.7918	0.7458	0.7073	0.6750	0.6475	0.6240	0.6037	0.5720	0.5456	0.5252	0.5088	0.4952	0.4744	0.4589	0.4469
0.0139	0.9060	0.7607	0.6692	0.6086	0.5661	0.5348	0.5109	0.4919	0.4764	0.4635	0.4428	0.4268	0.4138	0.4030	0.3936	0.3780	0.3653	0.3545
0.0278	0.7680	0.5997	0.5188	0.4714	0.4396	0.4161	0.3976	0.3824	0.3694	0.3581	0.3392	0.3234	0.3099	0.2981	0.2876	0.2694	0.2539	0.2406
0.0556	0.5817	0.4338	0.3699	0.3306	0.3025	0.2805	0.2625	0.2472	0.2340	0.2224	0.2029	0.1867	0.1732	0.1617	0.1515	0.1348	0.1215	0.1106
0.1111	0.3730	0.2575	0.2051	0.1721	0.1488	0.1313	0.1174	0.1063	0.0970	0.0893	0.0771	0.0680	0.0609	0.0552	0.0506	0.0436	0.0385	0.0346
0.1667	0.2445	0.1533	0.1132	0.0894	0.0735	0.0623	0.0538	0.0474	0.0423	0.0384	0.0325	0.0283	0.0255	0.0230	0.0211	0.0182	0.0162	0.0143
0.2222	0.1523	0.0854	0.0581	0.0426	0.0328	0.0261	0.0213	0.0177	0.0151	0.0133	0.0101	0.0081	0.0069	0.0055	0.0047	0.0031	0.0016	0.0005
0.2778	0.0798	0.0369	0.0206	0.0119	0.0061	0.0021	-0.0009	-0.0030	-0.0047	-0.0061	-0.0078	-0.0089	-0.0098	-0.0104	-0.0110	-0.0119	-0.0129	-0.0141
0.3333	0.0164	-0.0030	-0.0092	-0.0130	-0.0164	-0.0187	-0.0211	-0.0228	-0.0242	-0.0256	-0.0272	-0.0283	-0.0288	-0.0294	-0.0302	-0.0304	-0.0314	-0.0330
0.3889	-0.0468	-0.0414	-0.0384	-0.0375	-0.0386	-0.0408	-0.0430	-0.0451	-0.0468	-0.0486	-0.0509	-0.0525	-0.0540	-0.0540	-0.0561	-0.0557	-0.0569	-0.0577
0.4444	-0.1188	-0.0851	-0.0720	-0.0670	-0.0660	-0.0672	-0.0692	-0.0716	-0.0743	-0.0759	-0.0805	-0.0852	-0.0863	-0.0892	-0.0916	-0.0943	-0.0946	-0.0965
0.5	-0.2128	-0.1419	-0.1170	-0.1054	-0.1016	-0.1014	-0.1032	-0.1057	-0.1089	-0.1131	-0.1193	-0.1262	-0.1313	-0.1362	-0.1418	-0.1473	-0.1523	-0.1569

Table 5 Normalized COD parameter $V_b^{out}(\theta/\pi, R/t)$ under an in-plane bending stress

θ/π \ R/t	5	10	15	20	25	30	35	40	45	50	60	70	80	90	100	120	140	160
0.0056	0.6728	0.8924	0.8317	0.7809	0.7385	0.7029	0.6728	0.6472	0.6253	0.6064	0.5769	0.5523	0.5333	0.5181	0.5058	0.4868	0.4731	0.4626
0.0139	0.5289	0.7397	0.6635	0.6121	0.5758	0.5493	0.5289	0.5130	0.5001	0.4894	0.4728	0.4602	0.4503	0.4422	0.4354	0.4244	0.4158	0.4087
0.0278	0.4506	0.6024	0.5414	0.5053	0.4814	0.4641	0.4506	0.4397	0.4305	0.4227	0.4096	0.3989	0.3898	0.3819	0.3747	0.3625	0.3519	0.3426
0.0556	0.3671	0.4868	0.4432	0.4159	0.3960	0.3802	0.3671	0.3558	0.3458	0.3369	0.3213	0.3081	0.2966	0.2864	0.2772	0.2612	0.2477	0.2359
0.1111	0.2568	0.3810	0.3391	0.3107	0.2890	0.2715	0.2568	0.2444	0.2334	0.2238	0.2075	0.1939	0.1825	0.1728	0.1643	0.1504	0.1393	0.1302
0.1667	0.1931	0.3160	0.2730	0.2444	0.2232	0.2067	0.1931	0.1818	0.1721	0.1637	0.1498	0.1386	0.1298	0.1224	0.1162	0.1062	0.0988	0.0927
0.2222	0.1580	0.2733	0.2305	0.2034	0.1841	0.1696	0.1580	0.1486	0.1408	0.1340	0.1227	0.1144	0.1076	0.1019	0.0972	0.0898	0.0843	0.0800
0.2778	0.1415	0.2470	0.2051	0.1798	0.1629	0.1507	0.1415	0.1337	0.1275	0.1224	0.1136	0.1068	0.1010	0.0967	0.0926	0.0866	0.0824	0.0787
0.3333	0.1370	0.2344	0.1930	0.1694	0.1543	0.1446	0.1370	0.1309	0.1264	0.1221	0.1154	0.1100	0.1054	0.1024	0.0985	0.0936	0.0892	0.0858
0.3889	0.1419	0.2351	0.1927	0.1703	0.1567	0.1479	0.1419	0.1376	0.1341	0.1314	0.1267	0.1234	0.1201	0.1163	0.1133	0.1096	0.1062	0.1039
0.4444	0.1557	0.2504	0.2050	0.1816	0.1684	0.1609	0.1557	0.1529	0.1508	0.1507	0.1476	0.1453	0.1447	0.1433	0.1430	0.1403	0.1380	0.1371
0.5	0.1798	0.2849	0.2323	0.2062	0.1920	0.1841	0.1798	0.1774	0.1762	0.1770	0.1781	0.1801	0.1826	0.1846	0.1878	0.1891	0.1910	0.1931

Table 6 Stresses at the sodium surface of advanced loop typed LMFR plant

Stress factors	Axial stress (MPa)
Internal pressure	11.9
Dead weight	19.1
Thermal distribution	75.0

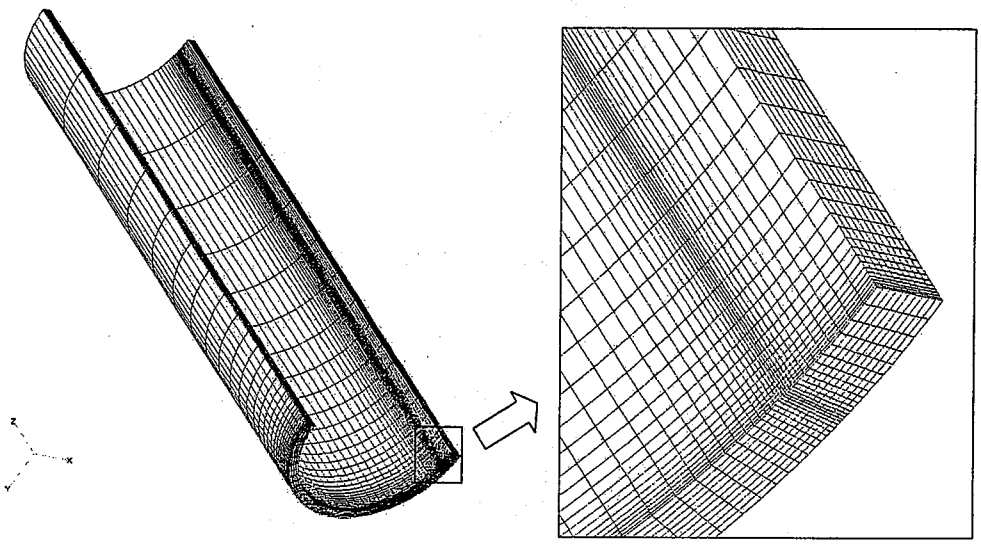

Fig.1 An example of FEM model (R/t=10, θ/π=0.0556)

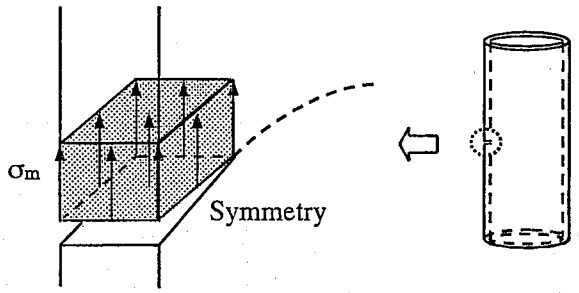

(a) Membrane stress only

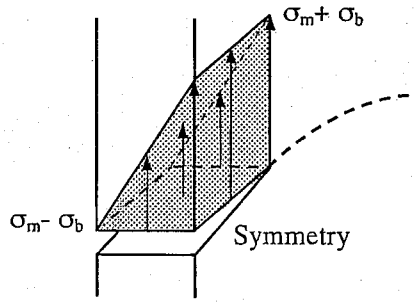

(b) Membrane and inner-surface plus-bending stresses

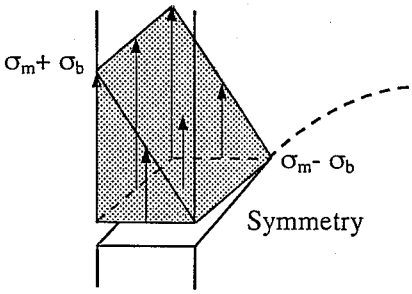

(c) Membrane and outer-surface plus-bending stresses

Fig.2 Schematic loading types

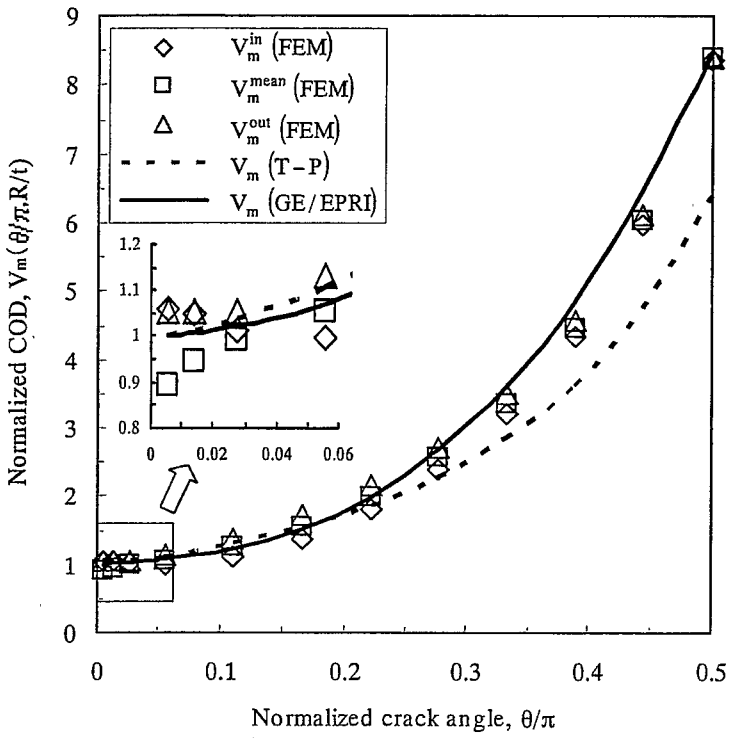

Fig.3 Comparisons of COD behaviors between FEM results and theoretical solutions (R/t=10)

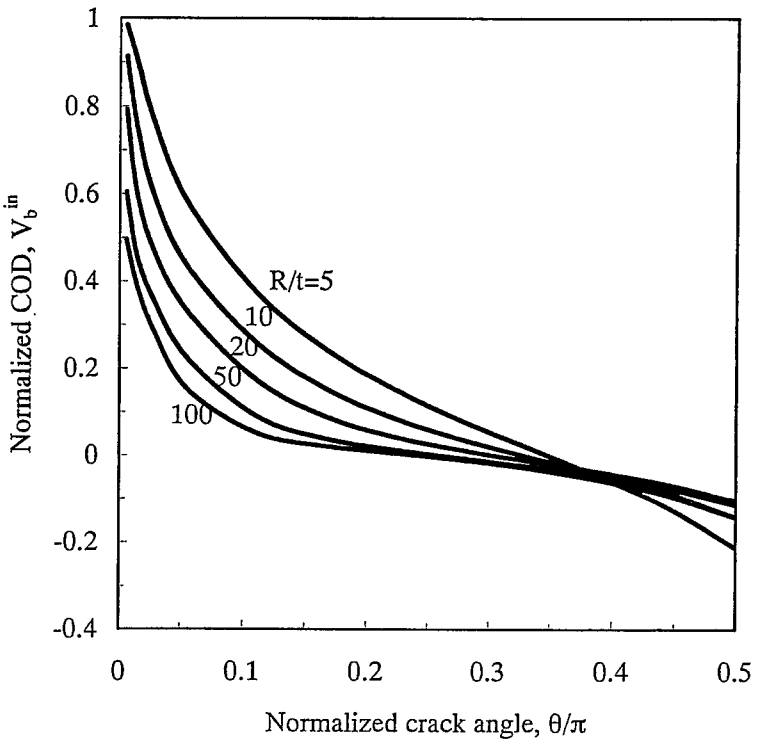

Fig.4 Crack opening behavior of inner-surface subjected to a plus-bending stress

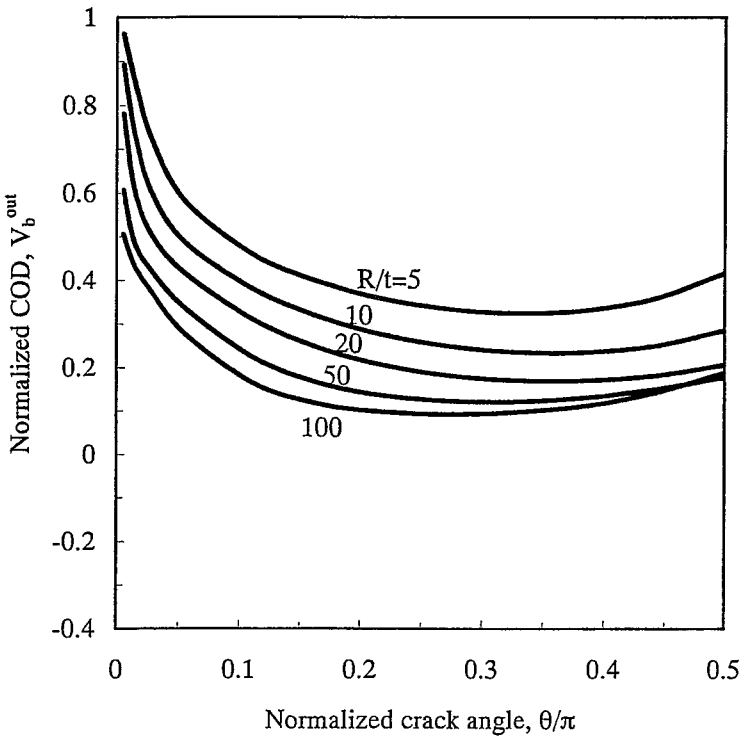

Fig.5 Crack opening behavior of outer-surface subjected to a plus-bending stress

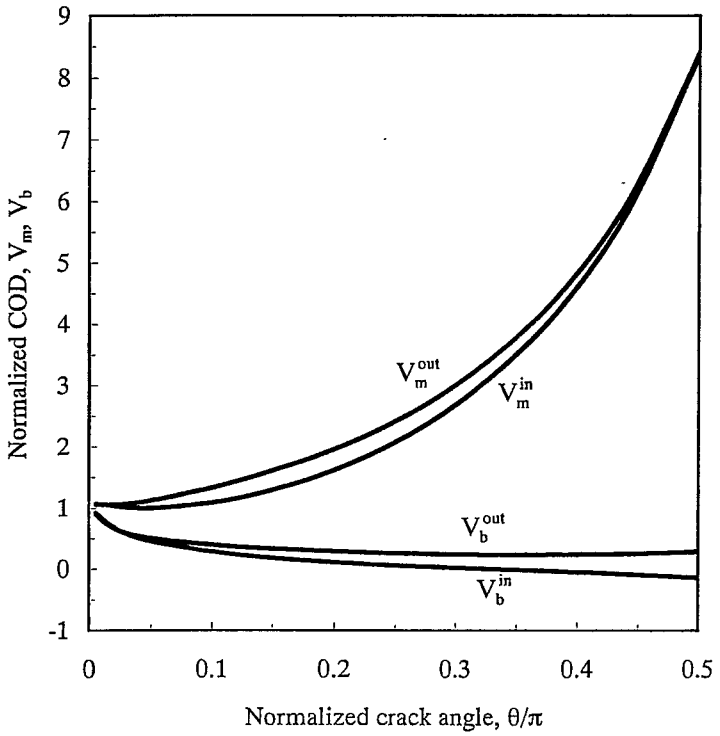

Fig.6 Crack opening behavior of inner and outer-surface subjected to a membrane or a plus-bending stress (R/t=10)

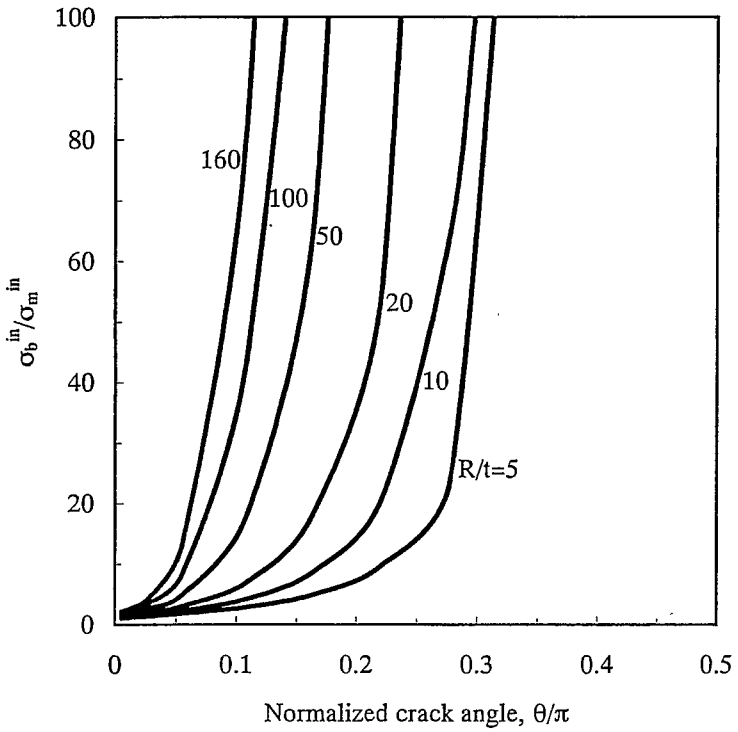

Fig.7 Ratio of an in-plane bending to membrane stress on same crack opening behaviors at inner-surface

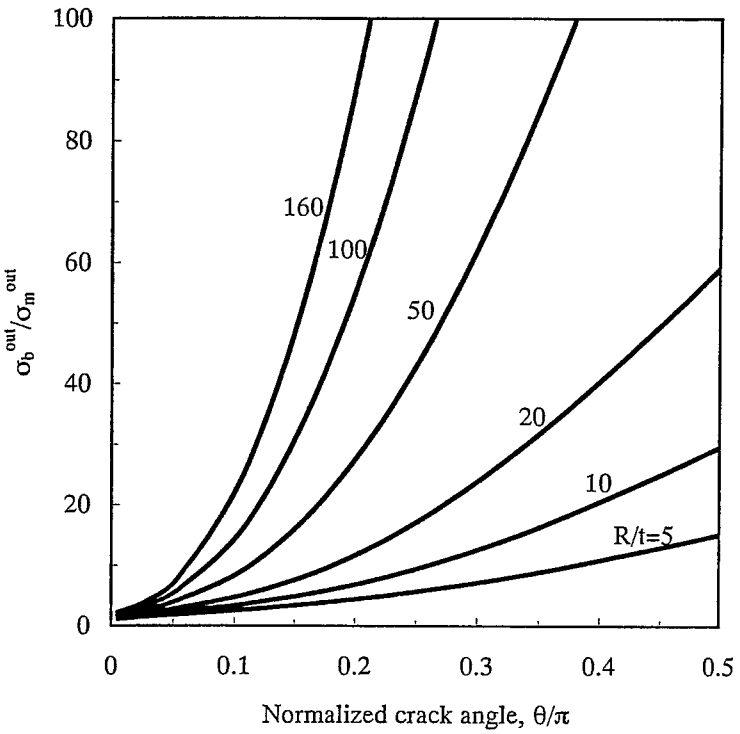

Fig.8 Ratio of an in-plane bending to membrane stress on same crack opening behaviors at outer-surface

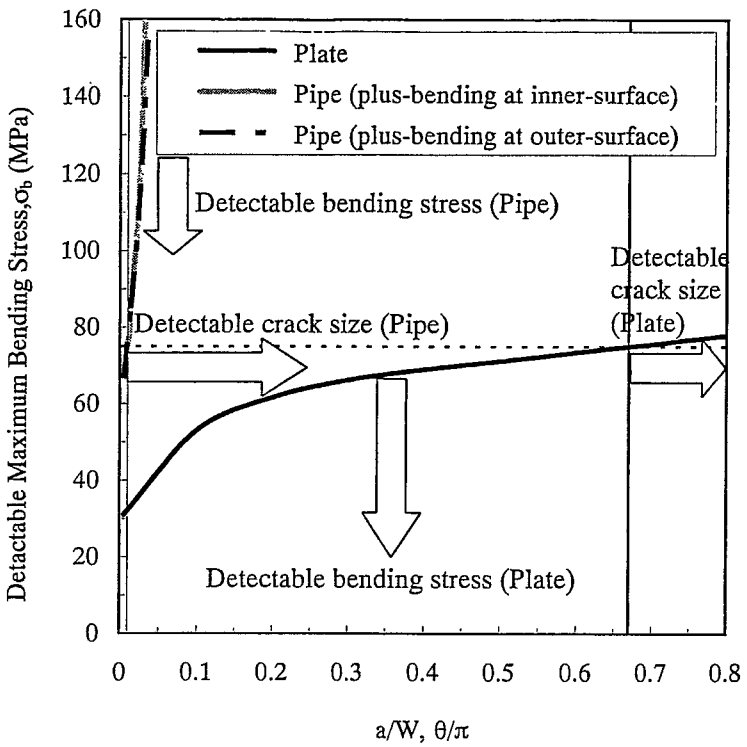

Fig.9 Detectable crack length at the sodium surface of advanced loop typed LMFR plant (σ_m = 31.0 MPa)